UNSTABLE NECK FORMATION AS A PRECURSOR TO DUCTILE FRACTURE DURING HIGH-RATE PLANAR EXTENSION

L. B. FREUND AND N. J. SØRENSEN
Division of Engineering, Brown University
Providence, R.I. 02912 USA

ABSTRACT

The phenomenon discussed is the bifurcation in deformation mode of a material undergoing homogeneous extension at high rate under plane strain conditions. The formation of diffuse necks as precursors to dynamic ductile fracture is of particular interest. The problem is first discussed within the context of the theory of bifurcation for incompressible, incrementally linear, rate-independent materials, with particular attention on the influence of material inertia on bifurcation conditions. This is followed by description of some results on neck formation at high strain rates obtained by finite element simulation of the rapid radial expansion of an elastic-viscoplastic ring under plane strain conditions. These simulations show that the first departure from uniform deformation occurs at the site of quasistatic neck formation, but this incipient neck grows too slowly to be significant. Instead, a critical mode of a much smaller wavelength is found somewhat later in the deformation history.

KEYWORDS

Bifurcation, strain localization, ductile failure, dynamic failure.

INTRODUCTION

During extension of a ductile plate or radial expansion of a ductile shell, deformation is often found to proceed more or less homogeneously within the plastic range until it is interrupted by the formation of localized necks or shear bands. These regions of localized deformation then typically evolve into ductile fractures. The focus here is on the formation of such necks during high rate extension of a plate or shell as a bifurcation phenomenon, and particularly on the influence of inertia on the stress level necessary for bifurcation.

To this end, a bifurcation problem is formulated for a rectangular block of an incompressible elastic-plastic material deforming at high rate under plane strain conditions. The block can be viewed as a segment of a plate or shell when symmetry is enforced. Opposite ends of the block are subjected to a uniform normal velocity V_0. The faces of the block are otherwise free of traction. The block initially undergoes a nearly homogeneous deformation, and the goal is to establish conditions on loading, geometry and material properties under which the homogeneous deformation can give way to a nonhomogeneous deformation with the

initial rate of deformation being large enough for these conditions to be influenced by material inertia.

Up to the instant of bifurcation, the deformation field throughout the material is essentially uniform. Material coordinates X_k referred to an underlying Cartesian basis are introduced in the reference configuration of the block, which is taken to occupy the region $-\ell_1 \leq X_1 \leq \ell_1$, $-\ell_2 \leq X_2 \leq \ell_2$. The dominant material velocity field referred to these coordinates is

$$v_1^0(X_1, X_2, t) = \frac{X_1 V_0}{\ell_1}, \quad v_2^0(X_1, X_2, t) = -\frac{X_2 V_0}{\ell_1 (1 + V_0 t/\ell_1)^2} \tag{1}$$

The imposed end velocity V_0 acts in the 1-direction, and the instantaneous stretching rate in the 1-direction is V_0/ℓ_1. The time at which the configuration coincides with the reference configuration is chosen arbitrarily as $t = 0$.

It is noteworthy that the deformation (1) cannot be maintained by a homogeneous state of uniaxial stress. The pathlines of material particles are curves in space with the curvatures of these paths varying in the 2-direction at any instant, which implies a nonuniform distribution of particle acceleration throughout the block. The equations enforcing the balance of linear momentum lead to the conclusion that the stress state is a homogeneous tension, say σ, in the 1-direction plus a hydrostatic pressure which varies in the 2-direction. In terms of components of Cauchy stress σ_{ij}, the distribution has the form $\sigma_{11} = \sigma - p_I$, $\sigma_{22} = -p_I$ and $\sigma_{12} = 0$. In terms of material coordinates in the reference configuration, the pressure p_I is

$$p_I(X_2) = \frac{\rho V_0^2}{\ell_1^2} \frac{\ell_2^2 - X_2^2}{(1 + V_0 t/\ell_1)^4} \tag{2}$$

where ρ is the material mass density.

A number of studies of the conditions for bifurcation of the elastic-plastic block under quasistatic imposed extension or compression have been reported. Hill and Hutchinson (1975) identified the regimes of behavior and ranges of moduli for which the governing equations are elliptic, parabolic or hyperbolic. They also calculated the spectrum of bifurcation stresses for symmetric and antisymmetric diffuse deformation modes. Young (1976) carried out a similar analysis for plane strain compression. Needleman (1979) extended the analysis for plane strain tension/compression to solids characterized by a flow rule with the plastic deformation rate not being normal to the flow surface. Recently, Benallal and Tvergaard (1995) examined the case of bifurcation of a block for a particular strain gradient plasticity theory. All of these analyses have been based on Hill's (1959, 1961) bifurcation theory for quasistatic deformation.

FIELD EQUATIONS

Consider once again the problem of plane strain extension of the block outlined in the Introduction. The constitutive equations for the incompressible, incrementally linear and time-independent materials under consideration here are written in terms of the Jaumann rate of Cauchy stress $\hat{\boldsymbol{\sigma}}$ and the rate of deformation $\mathbf{D}$ as

$$\hat{\sigma}_{11} = 2\mu^* D_{11} + \dot{p}, \quad \hat{\sigma}_{22} = 2\mu^* D_{22} + \dot{p}, \quad \hat{\sigma}_{12} = 2\mu D_{12} \tag{3}$$

The material parameters μ and μ^* appearing in (3) are the instantaneous moduli for simple shearing on the coordinate planes and on the planes inclined at 45° to the coordinate planes, respectively.

In the present analysis, the focus is on elastic-plastic materials with parameters in the interval $0 < \mu/\mu^* < \frac{1}{2}$. (Note that for a hypoelastic-plastic material $\mu = \frac{1}{3}E_s$ and $\mu^* = \frac{1}{3}E_t$ where E_s and E_t denote the secant and tangent moduli, respectively, of the uniaxial tensile stress–strain curve. For the case of a material described by a (piecewise) power hardening law, μ^*/μ is the strain hardening exponent (cf. Tvergaard, Needleman and Lo (1981)).

Elimination of the hydrostatic stress rate $\dot{p}$ leads to the form of the constitutive equations used by Hill and Hutchinson (1975), that is,

$$\hat{\sigma}_{11} - \hat{\sigma}_{22} = 2\mu^* (D_{11} - D_{22}), \quad \hat{\sigma}_{12} = 2\mu D_{12} \tag{4}$$

Incompressiblilty is assured if

$$D_{11} + D_{22} = 0 \tag{5}$$

The balance of momentum is conveniently expressed in terms of the nominal stress $\mathbf{s}$, which is related to the Cauchy stress $\boldsymbol{\sigma}$ by

$$\mathbf{F} \cdot \mathbf{s} = \boldsymbol{\sigma} \tag{6}$$

where the deformation gradient $\mathbf{F}$ is constrained by the condition $\det \mathbf{F} = 1$ in light of (5). The momentum balance can be written in component form relative to the Cartesian material frame X_i as

$$s_{ij,i} = \rho \ddot{u}_j \tag{7}$$

where u_j is the material displacement, ρ is the material mass density, the comma denotes differentiation with respect to X_i at fixed t, and the superposed dot denotes differentiation with respect to t at fixed values of X_i. The incremental form of (7) for the incompressible material is

$$\dot{s}_{ij,i} = \rho \dot{v}_j \tag{8}$$

where $v_j(X_1, X_2, t)$ is the material particle velocity.

Here, the attention is on the possible onset of a spatially *nonuniform* deformation field as a bifurcation from the velocity field (1) at a current configuration which represents some fully developed advanced stage of deformation. A useful simplification of the boundary value problem formulation is obtained by choosing the current configuration, whose state is being interrogated, as the reference configuration and by choosing the time scale so that the system is in this configuration at $t = 0$, as has been done in (1). Thus, the velocity field (1) evaluated at $t = 0$ is that of both the current and reference configurations, and $\mathbf{F}$ is the unit or identity tensor. All equations can be satisfied by continuing homogeneous deformation beyond the reference configuration as in (1). However, the goal is to seek conditions for which the governing equations can also be met for a continuing deformation beyond the reference configuration which is not homogeneous. For this choice of reference configuration, $\mathbf{s} = \boldsymbol{\sigma}$ instantaneously and the increments in nominal stress and Cauchy stress are related by

$$\dot{\mathbf{s}} = \dot{\boldsymbol{\sigma}} - \boldsymbol{\Gamma} \cdot \boldsymbol{\sigma} + \boldsymbol{\sigma} \mathrm{tr}(\mathbf{D}) \tag{9}$$

where $\boldsymbol{\Gamma}$ is the spatial velocity gradient and the Jaumann rate of Cauchy stress is

$$\hat{\boldsymbol{\sigma}} = \dot{\boldsymbol{\sigma}} - \boldsymbol{\Omega} \cdot \boldsymbol{\sigma} + \boldsymbol{\sigma} \cdot \boldsymbol{\Omega} \tag{10}$$

where the spin Ω is the antisymmetric part of the velocity gradient.

Following the analysis of Hill and Hutchinson (1975), the rate of momentum equation (8) can be reduced to the form

$$(\dot{s}_{11} - \dot{s}_{22})_{,12} + \dot{s}_{21,22} - \dot{s}_{12,11} = \rho\,(v_{1,1} - v_{2,2}) \tag{11}$$

Likewise, the constitutive equations (4) can be recast in the form

$$\dot{s}_{11} - \dot{s}_{22} = \left[2\mu^* - \tfrac{1}{2}\,\sigma\right](v_{1,1} - v_{2,2}) \tag{12}$$

$$\dot{s}_{12} = \left[\mu + \tfrac{1}{2}\,\sigma\right] v_{2,1} + \left[\mu - \tfrac{1}{2}\,\sigma + p_I\right] v_{1,2} \tag{13}$$

$$\dot{s}_{21} = \left[\mu - \tfrac{1}{2}\,\sigma + p_I\right] v_{2,1} + \left[\mu - \tfrac{1}{2}\,\sigma\right] v_{1,2} \tag{14}$$

Here σ is the uniform uniaxial stress acting in the 1-direction and p_I is the hydrostatic pressure given in (2). The fields satisfying these equations are subject to the boundary conditions

$$v_1 = 0 \quad \text{at} \quad X_1 = \pm\ell_1 \tag{15}$$

$$\dot{s}_{12} = 0 \quad \text{at} \quad X_1 = \pm\ell_1\,, \qquad \dot{s}_{21} = 0 \quad \text{and} \quad \dot{s}_{22} = 0 \quad \text{at} \quad X_2 = \pm\ell_2 \tag{16}$$

The condition (15) is the kinematic boundary condition on the velocity field, and the conditions (16) expressed in terms of rate of nominal stress are the natural boundary conditions on the velocity field.

As shown by Hill and Hutchinson (1975), the symmetry of the equations (12)-(14) is such that they can be combined in the variational equation

$$\dot{s}_{ij}\delta v_{j,i} = \delta U\,, \quad U = \tfrac{1}{2}\dot{s}_{ij}v_{j,i} \tag{17}$$

subject to the incompressibility condition. It must be understood in writing (17) that the nominal stress rate depends on velocity only through its linear variation with velocity gradient and that the variation represented by δ is a variation of velocity gradient.

The governing equations of the linear rate problem being considered here can also be recast in the context of a variational principle as $\delta\Phi = 0$ where

$$\Phi[v_i] = \int_{t_1}^{t_2}\int_{A_X}\left[\tfrac{1}{2}\dot{s}_{ij}v_{j,i} - \tfrac{1}{2}\rho\dot{v}_i\dot{v}_i\right] dX_1\,dX_2\,dt \tag{18}$$

where A_X is the area of the plane occupied by the block in its reference configuration and the times t_1, t_2 are arbitrary. Again, the nominal stress rate is assumed to depend on velocity only through its linear dependence on velocity gradient and the δ implies a variation in velocity which is arbitrary except that it must vanish on any part of the boundary of A_X on which kinematic boundary conditions are imposed, as well as at times $t = t_1$ and $t = t_2$.

It is obvious that the functional

$$\int_{A_X}\rho\dot{v}_i\dot{v}_i\,dX_1\,dX_2\,dt > 0 \tag{19}$$

is positive for all admissible velocity fields. In analogy with the linear theory of elasticity, the uniqueness of the incrementally linear rate problem is therefore assured if

$$\int_{A_X} U\,dX_1\,dX_2\,dt > 0 \tag{20}$$

The coefficients in the constitutive equations (12)-(14) are different from those in the quasistatic case because of the pressure p_I. Thus, the failure of the inequality (20) can be expected to occur under different conditions in the dynamic case, in general, than the conditions for bifurcation in the quasistatic case. Hutchinson's (1974) sufficiency criterion for quasistatic bifurcation of a plastic solid with a smooth yield surface under multiaxial stress states would be unaffected by the additional hydrostatic pressure due to inertia since stress measures entering this criteria are deviatoric. Thus, a possible dynamic bifurcation from the uniform velocity field (1) differs from the quasistatic bifurcation because of the different constitutive coefficients or because other types of restrictions arise from the high velocities in the background motion (1). Obviously, the coefficients in the constitutive equations (4) reduce to the coefficients relevant for the quasistatic case for rectangular blocks with a large aspect ratio since the effect of lateral inertia as given by (2) vanishes with the square of the aspect ratio of the block. It is noteworthy that the classification into elliptic, parabolic and hyperbolic regimes of the dynamical incremental field equations *without* the hydrostatic pressure due to lateral inertia is identical to the classification reported by Hill and Hutchinson (1975) for the quasistatic case. The neck bifurcation modes are thus also relevant for the dynamic extension of a block with a large aspect ratio, as long as these modes are otherwise admitted by the dynamic nature of the problem.

NECKING AND ONSET OF FAILURE IN DYNAMICALLY EXPANDING RINGS

In order to demonstrate some effects of inertia on high strain rate elastic-plastic deformation processes of relevance to engineering applications, results of simulation of steel rings expanding radially under plane strain conditions due to dynamic loading are included. The rings have an initial radius of $R_0 = 0.07\,\text{m}$ in all cases, and an initial thickness-to-radius ratio of $h_0/R_0 = 1/35,\ 1/70$ or $1/140$. The impact is specified as a uniformly distributed body force acting in the radial direction. The time evolution of the body force is taken to follow a sine curve, so that the amplitude is zero after half a period, which is defined as the impact time. Inertia imparted to the material continues to drive the deformation thereafter. The wall thickness is assumed to have an imperfection in the form of a periodic variation in half-thickness $\Delta h_0(\theta) = \xi h_0 \cos 8\theta$ where θ is the angular position along the ring (i.e. the initial wall thickness is $h_0 + 2\Delta h_0$). The resulting deformation is assumed to be periodic and only a segment of 22.5° is analyzed. Fig. 1 shows results of an impact simulation for a ring with $h_0/R_0 = 1/70$ in terms of contours of constant effective plastic strain, contours of constant void volume fraction and contours of constant temperature (in C°) at an instant where the overall hoop strain is approximately 0.65. As seen from the figure multiple necking has occured and failure is developing in several of these necks.

Fig. 2 shows the nominal hoop stress T at $\theta = 0°$ normalized by the yield strength σ_0 versus the hoop nominal strain $\Delta R/R_0$. Two pairs of curves are shown corresponding to thickness imperfections $\xi = 0$ and 0.01 and strain-rate-hardening exponents of $m = 0.001$ and 0.002. When $\xi = 0$, there is no necking in the ring segment within the range of overall straining studied here. With a (relatively large) imperfection amplitude present in the ring, necking occurs at a somewhat smaller overall strain for the material with the smaller strain rate hardening exponent. The impact time of 12.2 ms is relatively long and a single neck is developed in this case, exactly as in a quasistatic analysis.

The simulations were based on a dynamic finite element procedure (e.g., see Knoche and Needleman, 1993) with an internal variable dilatant viscoplastic material model used to

describe the ductile failure by void nucleation, growth and coalescence (cf. Gurson (1977), Tvergaard (1990)). In the present implementation of the Gurson model, both strain-controlled and stress-controlled void nucleation can be taken into account. However, to avoid large-scale computations, only strain-controlled nucleation was used in the present case. Also, thermal softening by adiabatic heating has been taken into account.

The material data used in the simulations (except for the results in Fig. 2) correspond to a ductile pressure vessel steel (denoted pvs in the following) which has been characterized by Naus *et al.* (1988).

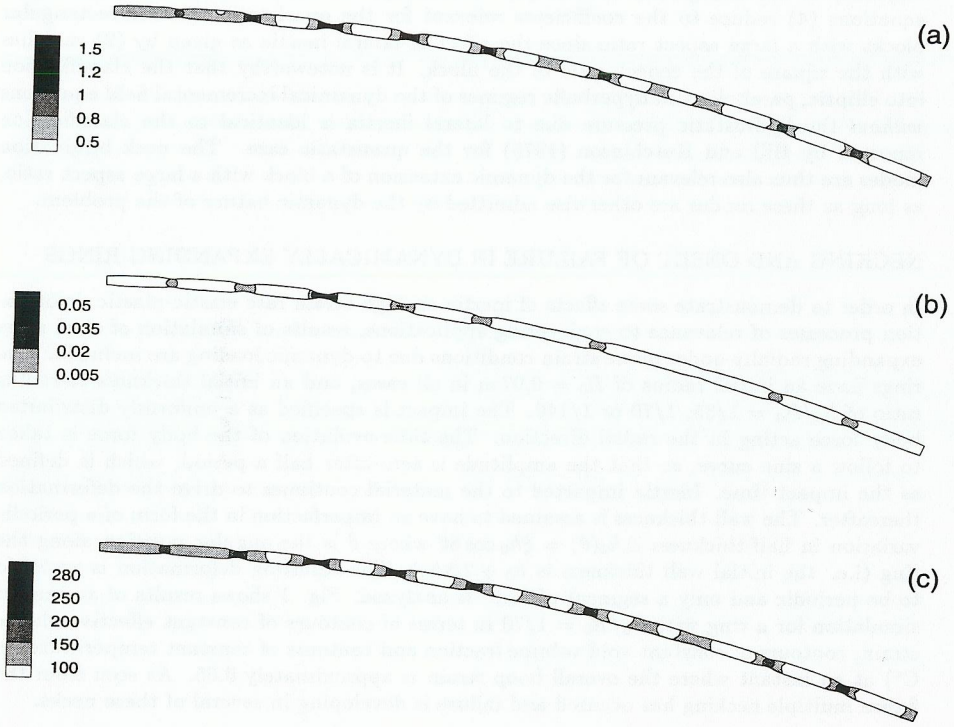

Figure 1. Contours of constant (a) effective plastic strain, (b) void volume fraction, and (c) temperature in °C for a pvs-steel ring with $h_0/R_0 = 1/70$ deformed to $\Delta R/R_0 = 0.65$ by a body force impact with amplitude $F = 10^8$ N/kg and impact time equal to 10 μs. The ring is initially thinnest at the extreme left end and thickest at the right end in the figure ($\xi = 0.01$).

The failure process in the pvs steel can be described within the context of the Gurson model by both strain-controlled and stress-controlled void nucleation since the behavior of this steel is consistent with two families of precipitate particles where the strain-controlled failure process is associated with the smaller of these particles and stress controlled void nucleation is associated with the larger particles. The use of the strain-controlled failure initiation or no failure mechanism at all restricts consideration to the process of dynamic necking in steel rings. Some of the relevant data for the pvs steel ring as used here are the strain hardening exponent $N = 0.1$, the strain rate hardening exponent $m = 0.002$, the room temperature yield strength $\sigma_0 = 426$ MPa, the material mass density $\rho = 7850\,\mathrm{kg/m^3}$, the starting temperature 20°C, the coefficient of thermal expansion $\beta = 1.1\times10^{-5}/°\mathrm{C}$, the fraction of plastic work converted into heat $\chi = 0.9$, the elastic modulus $E = 206.9$ GPa, the Poisson ratio $\nu = 0.3$ and the volume fraction of strain-controlled void nucleating particles $f_v = 0.002$.

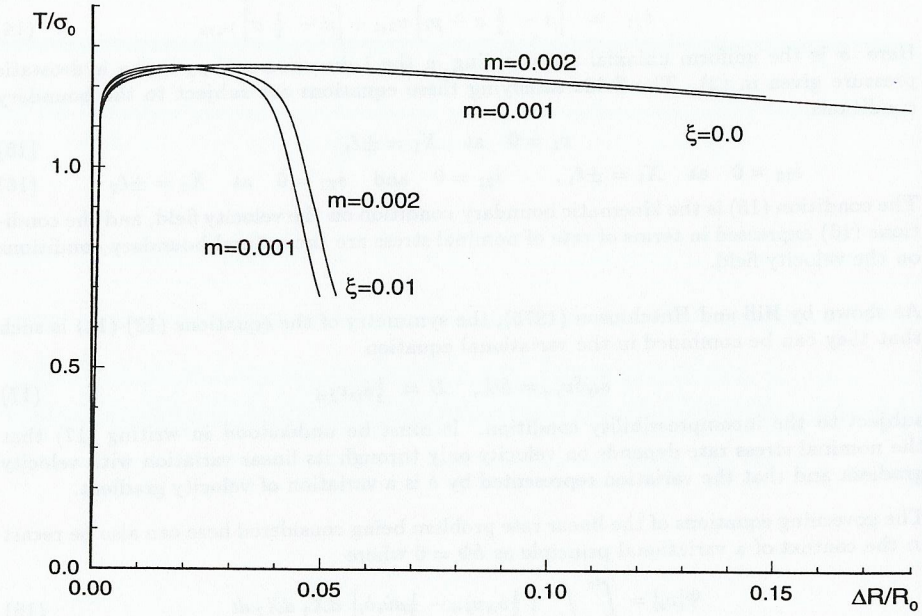

Figure 2. The effect of rate-dependency on the impact behavior in rings without imperfection $\xi = 0.0$ and with imperfection $\xi = 0.01$ for a slow impact (12.2 ms). The copper data from the analysis by Han and Tvergaard (1995) has been used in this case.

A study of dynamic necking in rings has been conducted recently by Han and Tvergaard (1995) using a rate-independent plasticity model. The present computations have been carried out along the same lines; for details on boundary conditions the reader is referred to this study. The results described in Fig. 2 have also been compared to the results of Han and Tvergaard (1995), which corresponds to the limit $m \to 0$. The results suggest that, whereas the strain-rate-hardening effects may play a significant role in delaying the onset of necking compared to the rate independent case, they become very significant for the delay in necking observed in the dynamic case when the standard power-low type of dependency is assumed. However, the phenomenon of multiple necking observed by Han and Tvergaard (95) for a rate-independent material and found here for a slightly rate-dependent material are very similar, suggesting that strain-rate-hardening effects play a

secondary role compared with the imperfection sensitivity of the viscoplastic material in the process of neck formation.

In order to visualize the sequence of events in the process of dynamic necking, an average effective plastic strain rate over a cross-section, normalized by the average strain rate $\dot{R}/R$, has been used. Typically, the average strain rate in these calculations has increased to a value somewhat less that 10^4/s at the time the impact loading on the ring ceases, and it then decays as the rate of expansion of the ring gradually diminishes. This normalized average plastic strain rate $\dot{e}_s(\theta, t)$ provides a useful instantaneous measure of the deviation from uniform deformation.

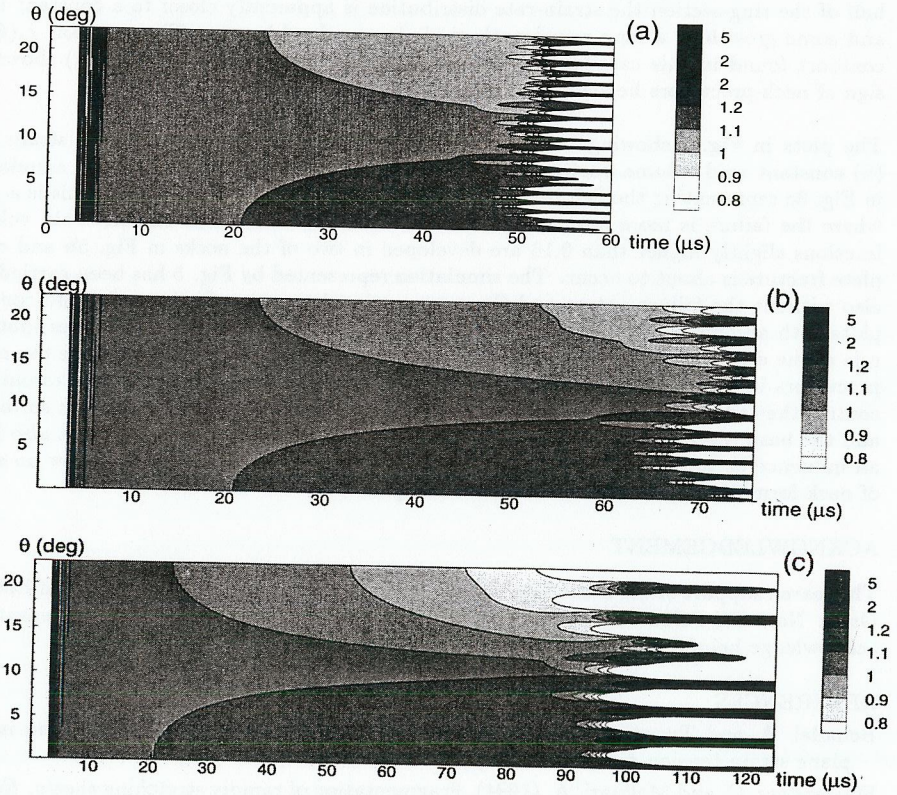

Figure 3. Deformation history represented in terms of contours of constant values of the normalized cross-sectional effective plastic strain rate $\dot{e}_s$ over the θ, t-plane for rings of the pvs-steel with the initial thickness-to-radius ratio being equal to (a) 1/140 (b) 1/70 and (c) 1/35. The impact time is 10 μs and the body force amplitude is 10^8 N/kg in all cases.

This normalized cross-sectional plastic strain rate is recorded over the entire deformation history. Results in the form of contours of $\dot{e}_s(\theta, t)$ in the θ, t-plane are shown in Fig. 3 for three impact simulations representing rings with different thickness-to-radius ratios.

Viewed in this way, the darker shading shows plastic strain rates which are higher than the average strain rate, and lighter shading shows plastic strain rates which are smaller than the average strain rate. For all cases, the strain rate distribution around the circumference is found to be nearly uniform at the time when the impact loading is completely removed, i.e., after 10μs. Initial loading through the elastic deformation regime gives rise to a vibration with nodes close to the midpoints of the intervals between the thickest and the thinnest points on the ring. With the onset of plastic deformation, this vibration dies out and accordingly the plastic loading-elastic unloading associated with this vibration also dies out.

After the applied load is completely removed, inertia continues to drive the deformation, which is nearly uniform for the three cases in Fig. 3, until the time is approximately two times the impact time (i.e. 20 μs). In all cases, a slightly higher strain rate is found at the thinnest point of the ring shortly after 20 μs and this higher strain rate region grows in size thereafter. Almost simultaneously, a strain rate slightly smaller than average is visible at the thicker part of the ring. Even with higher resolution in the contour plots than can be represented here, this pattern with a higher-than-average strain rate region forming at the site of the imperfection and slowly growing in size but with a constant intensity thereafter seems to be common to all cases.

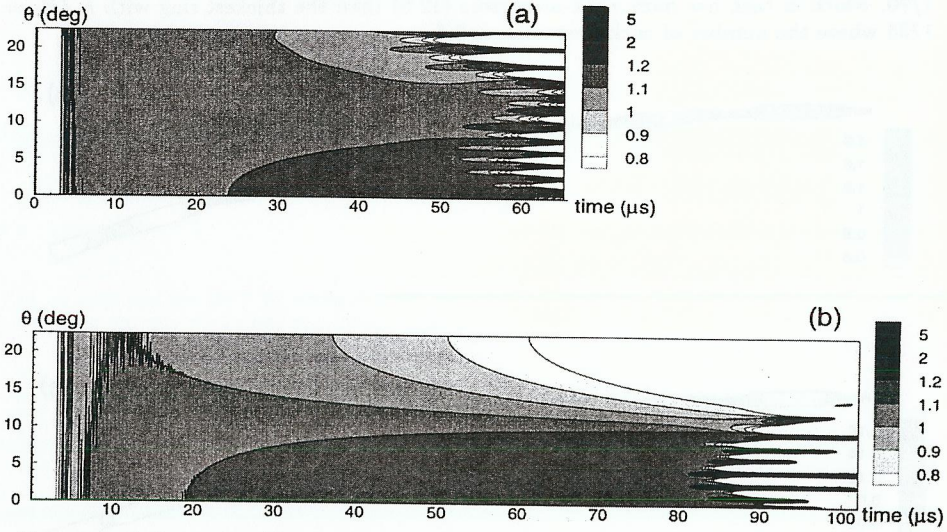

Figure 4. Deformation history represented in terms of contours of constant values of the normalized cross-sectional effective plastic strain rate $\dot{e}_s$ over the θ, t-plane for rings of pvs-materials, but with the strain hardening exponent equal to (a) $N = 0.02$ and (b) $N = 0.25$. The impact time is 10 μs, the body force amplitude is 10^8 N/kg in all cases and $h_0/R_0 = 1/70$.

In the context of the bifurcation results for a quasistatic plane strain tension test, this situation can be described qualitatively as slow growth of the long wavelength mode which, in the quasistatic case, would lead to a neck developing symmetrically near 0° and extending

to a few degrees to either side of this point. However, except from the slowly growing long-wavelength mode, the three cases in Fig. 3 show rather different behavior from the quasistatic case, in that multiple, closely spaced high/low strain rate zones are seen to develop for the dynamic cases analyzed here. The order of appearance of these high/low strain rate zones is not the same for the three cases and the intensity varies. These short wavelength, highly non-uniform plastic strain rate patterns do not all develop into necks with equal strain intensity. However, this mode appears to be the *critical mode* in the sense that some of these *neck-precursors* do develop into macroscopic necks that are visible in contour plots like those in Fig. 1 which corresponds to the final deformation state for the history plot in Fig. 3b. It is worth noting that some of the neck-precursors corresponding to the critical mode shown Fig. 3 die out and the strain levels in the necks in Fig. 1 varies accordingly.

The distance between the neck-precursors in the critical mode varies along the section. Thus, for the ring with the initial aspect ratio 1/70 in Fig. 3b, the distance between the neck-precursors is 1.8° near $\theta = 0°$ and 2.0° near $\theta = 22.5°$. This is in accordance with the behaviour of necking modes in the quasistatic case where the distance between the necks varies with the thickness. For the case of the thinnest ring ($h_0/R_0 = 1/140$), Fig. 3a shows a larger number (20) of neck-precursors over the ring section than the ring with $h_0/R_0 = 1/70$, which in turn has more neck-precursors (12.5) than the thickest ring with $h_0/R_0 = 1/35$ where the number of neck-precursors is 7.5.

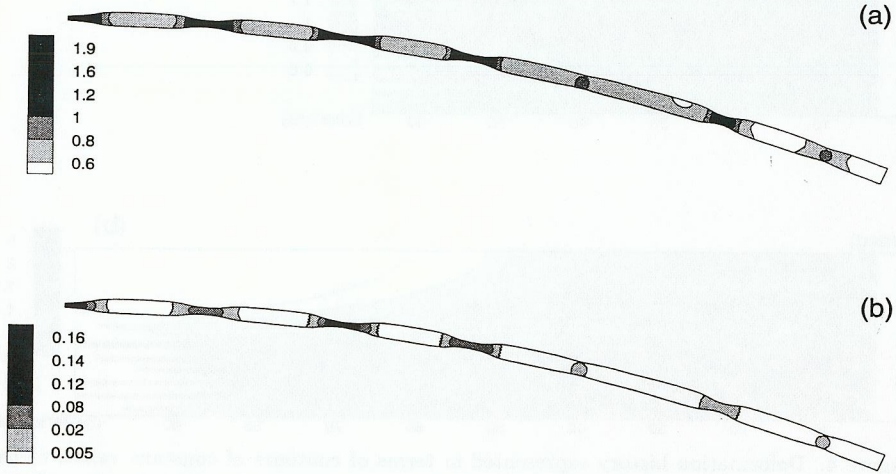

Figure 5. Contours of (a) constant effective plastic strain and (b) constant void volume fraction in a ring of pvs-steel with $h_0/R_0 = 1/35$ deformed to $\Delta R/R_0 = 0.44$. Impact time is 10 μs and the body force amplitude is 10^8 N/kg. The ring is initially thinnest at the extreme left end and thickest at the right end in the figure ($\xi = 0.01$).

To indicate the influence of the strain hardening parameter N, contours of normalized

cross-sectional average strain rate $\dot{e}_s(\theta, t)$ are shown in Figs. 4a and 4b for $N = 0.02$ and 0.25. This parameter has a large influence on the bifurcation stress in the quasi-static, rate-independent limit. Modest changes in the value of the strain hardening parameter have little influence on the spacing of neck-precursors. The case in Fig. 4a with the lower hardening value of 0.02 shows the development of two groups of neck-precursors, where the first group develops in the thicker region of the ring segment and the second group develops in the thinner portion. With $N = 0.25$, the combination of the large imperfection amplitude $\xi = 0.01$ and the high hardening exponent does not allow the deformation to enter a state with a strain-rate as close to uniform throughout the ring as in the other cases reported here, and some wave phenomena are seen more clearly in this case. In the lower half of the ring-section the strain-rate distribution is apparently closer to a constant level and some growth of a long wavelength mode is seen in this case. The constant $\dot{e}_s(\theta, t)$-contours found in this case (even when many more contour levels are chosen) shows no sign of neck-precursors beyond approximately 15°.

The plots in Fig. 5 showing contours of (a) constant effective plastic plastic strain and (b) constant void volume fraction correspond to the situation at the end of the simulation in Fig. 3c representing the deformation of the thickest ring ($h_0/R_0 = 1/35$). This is a case where the failure is more pronounced than in the situations shown earlier. Void volume fractions slightly higher than 0.16 are developed in two of the necks in Fig. 5b and complete fracture is about to occur. The simulation represented by Fig. 5 has been carried out also without the failure option and the cross-sectional average plastic strain rate contour plots with and without the failure model are essentially identical. This indicates that the role of the dilatant plasticity model is of minor importance in the process where the neck-precursors in Fig. 3c develop into full necks. The constitutive features which essentially control the failure evolution accounted for here can thus only be the adiabatic softening and the basic viscoplastic material response. In addition, the imperfection must also have an influence because simulations of the ring impact for the case with $\xi = 0$ show no signs of neck formation up to a mean hoop strain equal to 1.

ACKNOWLEDGEMENT

The rearch support of the Basic Engineering Sciences Division, U. S. Department of Energy, Grant No. DE-FG02-95ER14561, is gratefully acknowledged. It is also a pleasure to acknowledge helpful discussions of this work with Professor Alan Needleman.

REFERENCES

Benallal, A. and Tvergaard, V. (1995), Nonlocal continuum effects on bifurcation in the plane strain tension-compression test, *J. Mech. Phys. Solids* , **43**, 741-770.

Fressengeas, C. and Molinari, A. (1994), Fragmentation of rapidly stretching sheets, *Europ. J. Mech. A/Solids* ,**13** , 251-268.

Grady, D. E. (1987), Fragmentation of rapidly expanding jets and sheets, *Int. J. Impact Engrg.*, **5**, 285-292.

Gurson, A. L. (1977), Continuum theory of ductile rupture by void nucleation and growth - Part. I. Yield criteria and flow rules for porous ductile media, *J. Eng. Matr. Tech.*, **99**, 2-15.

Han, J. and Tvergaard, V. (1995), Effect of inertia on the necking behavior of ring specimens under rapid radial expansion, *Europ. J. Mech. A/Solids*, **14**, 287-307.

Hill, R. (1958), A general theory of uniqueness and stability in elastic-plastic solids, *J. Mech. Phys. Solids*, **6**, 236-249.

Hill, R. (1961), Bifurcation and uniqueness in non-linear mechanics of continua, in *Problems of Continuum Mechanics* , N. I. Muskhelishvili Volume, SIAM, Philadelphia, 155-164.

Hutchinson, J. W. (1974), Plastic buckling, in *Advances in Applied Mechanics*, edited by C. S. Yih, Academic Press, New York, **14**, 67-144.

Hutchinson, J. W. and Miles, J. P. (1974), Bifurcation analysis of the onset of necking in an elastic/plastic cylinder under uniaxial tension, *J. Mech. Phys. Solids*, **22**, 61-71.

Hutchinson, J. W. and Neale, K. W. (1978), Sheet necking-II. Time-independent behavior, *Mechanics of Sheet Metal Forming*, Plenum Press (General Motors Research Laboratories Symposium, 1977), 127-153.

Hutchinson, J. W. and Tvergaard, V. (1981), Shear band formation in plane strain, *Int. J. Solids Struc.*, **17**, 451-470.

Hutchinson, J. W. and Neale, K. W. (1977), Influence of strain rate sensitivity on necking under uniaxial tension, *Acta Met.*, **25**, 839-846.

Knoche, P. and Needleman, A. (1993), The effect of size on ductility of dynamically loaded tensile bars, *Europ. J. Mech. A/Solids*, **12**, 585-601.

Naus, D. J., Keeney-Walker, J., Bass, B. R., Fields, R. J., De Wit, R. and Low III, S. R. (1989), High-temperature crack-arrest behavior in 152-mm-thick SEN wide plates of quenched and tempered A533 grade B class 1 steel, NUREG/CR-5330 (ORNL/TM-11083), Oak Ridge National Laboratory, National Institute of Standards and Technology, April 1989.

Needleman, A. (1979), Non-normality and bifurcation in plane strain tension and compression, *J. Mech. Phys. Solids*, **27**, 231-254.

Needleman, A. (1991), The effect of inertia on neck development, *Topics in Plasticity*, Ed. by W. H. Yang, AM Press, Ann Arbor, Mi , 151-160.

Tugcu, P. and Neale, K. W. (1991), Deformation and plastic waves in dynamic tension tests, *Int. J. Solids Struc.*, **10**, 815-827.

Tugcu, P., Neale, K. W. and Lahoud, A. E. (1990), Inertial effects on necking in tension, *Int. J. Solids Struc.*, **11**, 1275-1285.

Tvergaard, V. (1990), Material failure by void growth to coalescence. *Advances in Applied Mechanics*, edited by John W. Hutchinson and Theodore Wu, Academic Press, New York, **27**, 83-151.

Tvergaard, V., Needleman, A. and Lo, K. K. (1981), Flow localization in the plane strain tensile test, *J. Mech. Phys. Solids*, **29**, 115-142.

Young, N. J. B. (1976), Bifurcation phenomena in the plane strain compression test, *J. Mech. Phys. Solids*, **24**, 77-91.